On Electric Field Distribution and Temperature Rise Effect of High Power VLF Antenna

Xianqiang Li [1], Kedan Mao [2], Ao Wang [1], Ji Tian [1], and Wenchuang Zhou [1]

[1] School of Automation
Wuhan University of Technology, Wuhan, 430070, China
lxq@whut.edu.cn, WAO@whut.edu.cn

[2] Nuclear Power Institute of China, Chengdu, 610005, China
15382442567@163.com

Abstract ─ When a high-power very low frequency (VLF) communication system is in operation, the end of the antenna is in an alternating strong electric field environment. Due to dielectric loss, abnormal temperature rise may occur at the end of the antenna. To solve the problem, analysis on the electric field distribution and temperature rising effect at the end of the antenna is first carried out in this paper. The factors that affect the electric field distribution and temperature rising, including the amplitude and frequency of the excitation voltage, the diameter of the antenna conductor and the material properties of the outer sheath of the antenna, are studied in detail. A novel approach to improve the electric field distribution and to suppress temperature rising is proposed by designing a dielectric loss eliminator, and the effectiveness of the designed device is verified by simulation.

Index Terms ─ Dielectric loss eliminator, electric field, temperature field, VLF antenna.

I. INTRODUCTION

Very low frequency (VLF) communication systems have several attractive features including stable and reliable propagation, capability to penetrate seawater and soil and intrinsic rejection to ionospheric disturbance interference [1-3]. Therefore, the VLF communication systems have been widely developed for applications such as submarine communication, long-distance communication, mineral exploration, and geophysics [4-9]. Vehicle-mounted VLF communication systems, whose antenna are lifted by balloons, have gained most research interests in recent years due to their flexibility and mobility, high transmission efficiency, and minimum requirement of floor space [10,11].

However, when a high-power VLF communication system is in operation, the end of the antenna will be exposed in the environment with strong and highly-varying electric field, where abnormal temperature rise might occur due to dielectric loss on the outer sheath material of the antenna. This can lead to disastrous consequences such as antenna breaking and balloon escaping. Hence, it is of primary importance to investigate the electric field distribution and temperature rise effects at the end of antenna to ensure safe and reliable operation of the vehicle-mounted VLF communication systems.

In a vehicle-mounted high-power VLF communication system, if the balloon is utilized to lift the antenna to transmit signals, the electric field intensity near the end region of the antenna can be extremely high. If the local electric field intensity exceeds the air ionization field intensity, the air will be ionized and the corona discharge phenomenon will occur [12]. Corona discharge will cause additional power loss, radio interference, as well as noise interference. More severely, corona discharge can cause unexpected breakdown of the high-power VLF communication system. In addition, since the outer sheath and load-bearing materials at the end of the antenna, which are made of polymer composite materials, are exposed in an environment with high-amplitude alternating electric field, dielectric heating is likely to occur and it can cause the antenna fracture in certain extreme conditions. Especially for the balloon-lifting type high-power VLF communication system, the breaking of the antenna will lead to catastrophic consequences of the balloon disconnection.

At present, there is rare research on electric field distribution and temperature rise at the terminal of VLF antenna. In [13], The selection of insulators in station-type VLF arrays is studied. Since high-power VLF transmit antennas usually operate in high voltage and large current conditions, electrical insulation must be paid attention to. In [14], Liu carried out simulation analysis of the radiation characteristics of the VLF dual-tail antenna and the near-field characteristics of the airborne platform by establishing the electromagnetic theoretical model of the airborne VLF dual-tail antenna system, and the strong corona of single-tail antenna

Submitted On: February 21, 2021
Accepted On: April 29, 2021
https://doi.org/10.47037/2020.ACES.J.360610

communication problem was optimized. In [15], Liu used finite element simulation software to establish the model of the aircraft and the VLF launching system, so as to study the electromagnetic environment of the airborne dual towed antenna, the near-field radiation characteristics of the towed antenna, the internal electromagnetic field, as well as the distribution and value of induced current of the aircraft by simulation calculation. In [16], a new method for establishing an airborne VLF single/dual towed antenna system model was proposed. The electromagnetic radiation characteristics and impedance characteristics of single/ dual towed antennas were discussed by simulation calculations. It pointed out that the performance of dual towed antennas is better than single tow antenna. The electric field distribution of the insulator at the terminal of the VLF antenna is obtained by simulation modeling. The magnitude and distribution of the voltage and current on the VLF antenna are obtained through integration [17]. Yang [18] theoretically analyzed the mechanism of electric field distortion and high local field intensity at the terminal of VLF communication antenna. At the same time, the affecting factors are discussed. Zhou [19] introduced the generation mechanism of the corona of the VLF transmitting antenna, theoretically derived the calculation method of the corona voltage of the VLF transmitting antenna, and analyzed the influencing factors of corona voltage calculation under different operating conditions. The distribution characteristics of the electric field at the terminal of the VLF antenna are obtained by numerical calculation. The improvement measure is proposed to solve the problem of electric field distortion, and the effectiveness of the improvement measures is verified by simulation calculation. Meanwhile, the factors that affecting the distribution of electric fields are also studied [20]. Shi [21] simulated the VLF antenna array and constructed a minimum protection distance model for electromagnetic radiation hazards. Through numerical calculation, the variation law of the comprehensive field intensity value of the VLF antenna array near area with the transmission power and loading frequency was obtained. Finally, the accuracy of the simulation is verified by experiments. The temperature field at the terminal of the VLF antenna is theoretically analyzed, and the heating principle at the terminal of the VLF antenna is expounded, and the temperature variations at the terminal of the VLF antenna under different operating conditions were discussed through finite element simulation modeling [22].

To summarize the existing works, there are few studies on coupled electro-thermal field at the end of antenna, especially for high-power balloon-lift VLF communication systems. Therefore, it is of great significance to carry out research on the electric field distribution and the temperature rise at the end of the transmitting antenna of high-power VLF communication system and to take effective measures to improve the electric field distribution and suppress temperature rising.

In this work, the distribution characteristics of the electric field and temperature field at the end of high-power VLF antenna are studied separately. Hence, the factors that affect the electric field and temperature at the end of the VLF antenna are studied through simulation calculations. The measure to solve electric field distortion and temperature rise (Dielectric Loss Eliminator) are proposed and the effectiveness of the measures is verified. It provides a certain reference for the design of the antenna.

II. PRELIMINARIES

In this section, the composition of the VLF antenna structure is introduced. The electric field distribution and the temperature rise caused by the dielectric loss at the end of the VLF antenna are analyzed theoretically.

A. Structure of a VLF antenna

The complete antenna system is shown in Fig. 1. A floating balloon and a ground vehicle are connected at each end of the antenna. The floating balloon is used to lift the antenna for signal transmission. The ground vehicle is used for tethering the floating platform after retrieval and towing the floating platform during release. The 1~3 km VLF antenna connects the two and serves as a connection and signal radiation.

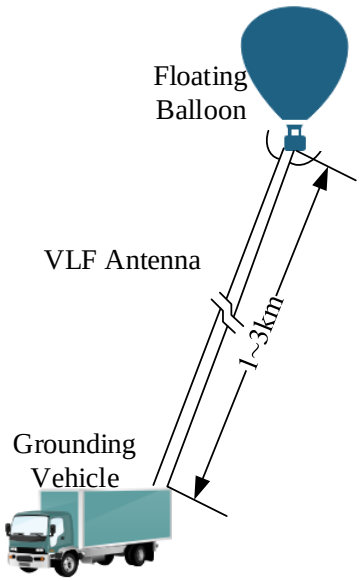

Fig. 1. Schematic diagram of antenna system.

As shown in Fig. 2, a typical VLF antenna is composed of four layers, including outer sheath, antenna conductor, inner sheath, and the aramid. Figure 2 (a) and Fig. 2 (b) present the sectional and vertical view of the

VLF antenna, respectively.

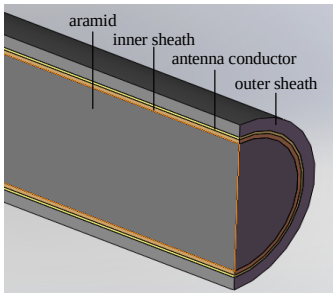

(a)

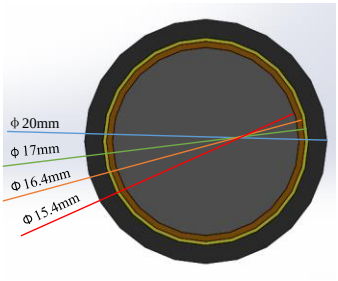

(b)

Fig. 2. Structure diagram of VLF antenna: (a) sectional view of the antenna; (b) vertical view of the antenna.

B. Electro-quasi-static equations

According to Faraday law of electromagnetic induction, the coulomb electric field E_q and the induced electric field E_i in the time-varying electric field are induced by electric charge q and varying magnetic field $\partial B/\partial t$ respectively. In the low-frequency electric field, if the induced electric field E_i is much lower than the coulomb field E_q, the $\partial B/\partial t$ term in the Maxwell's equations can be ignored. Hence, the time-varying electric field differential equation of the Maxwell's equations can be simplified to the electro-quasi-static Equations (1) – (4):

$$\nabla \times \boldsymbol{H} = \boldsymbol{J} + \frac{\partial \boldsymbol{D}}{\partial t}, \tag{1}$$

$$\nabla \times \boldsymbol{E} = 0, \tag{2}$$

$$\nabla \cdot \boldsymbol{B} = 0, \tag{3}$$

$$\nabla \cdot \boldsymbol{D} = \rho, \tag{4}$$

where, H is the magnetic field intensity, J is the conduction current density, E is the electric field intensity, B is the magnetic flux density, D is the electric displacement, and ρ is the charge density.

It can be seen from (1) – (4) that both the electrical quasi-static field and the electrostatic field have active and non-rotation in ignoring $\partial B/\partial t$, so the calculation method of the two fields is similar. In addition, the electric field intensity of the electric quasi-static field can also be expressed as the negative of the potential gradient, i.e.,

$$\boldsymbol{E} = -\nabla\varphi, \tag{5}$$

where φ is the potential function of the electric quasi-static field.

Therefore, it can be seen that the solutions of the electric quasi-static field and electrostatic field have a similar form. Furthermore, the conditions to be satisfied for inhomogeneous isotropic media are expressed using the constitutive relationships of media in the Maxwell's equations, i.e.,

$$\boldsymbol{D} = \varepsilon \boldsymbol{E}, \tag{6}$$

$$\boldsymbol{B} = \mu \boldsymbol{H}, \tag{7}$$

$$\boldsymbol{J} = \sigma \boldsymbol{E}, \tag{8}$$

where ε, μ, and σ represent the permittivity, permeability, and conductivity of the medium, respectively.

The Poisson equation satisfying potential $\varphi(t)$ can be obtained by substituting (5) and (6) into (4), i.e.,

$$\nabla^2\varphi = -\frac{\rho(t)}{\varepsilon}. \tag{9}$$

In summary, the electric field of the end of high-power VLF antenna is electric quasi-static field.

C. Theoretical analysis of dielectric loss

The temperature rise of the end of VLF antenna is caused by the existence of alternating electromagnetic fields [23]. Due to the polarization effects and dielectric loss, there are energy consumption and conversion processes in the outer sheath and load-bearing materials of the VLF antenna end. The outer sheath and load-bearing materials have a dielectric loss (mainly polarization loss) in the alternating electric field, which converts electrical energy into thermal energy. It causes a temperature rise at the end of the VLF antenna. According to the principle of dielectric loss, the energy loss per unit time and per volume can be calculated by:

$$W = \frac{\omega}{2}\varepsilon'' E_0^2, \tag{10}$$

$$\varepsilon'' = \varepsilon' \tan\delta, \tag{11}$$

$$\varepsilon' = \varepsilon_r \varepsilon_0, \tag{12}$$

where ε' and $\tan\delta$ can be obtained by consulting the data, ε_r is the relative dielectric constant, and ε_0 is the dielectric constant in vacuum.

Combining (10) – (12) yields the expression of dielectric loss energy W, i.e.,

$$W = \frac{\omega\varepsilon'}{2}(\tan\delta)\int_V |E_0|^2 \, dv. \tag{13}$$

It can be seen from (13) that, when the parameters of the material are constant, the dielectric loss energy W is proportional to the square of the electric field intensity. Hence, (13) relates the electric field to the dielectric loss

heating, and it fundamentally reveals the relationship between the electric field and the temperature field.

D. Heat transfer equations

Due to the dielectric loss, the antenna can be set as a heat source, and the heat generated in the medium can be obtained according to equation (13). The heat generated within the medium diffuses outward by heat conduction and convection. The heat conduction follows the equations (14),

$$\rho c \frac{\partial T(\vec{r},t)}{\partial t} - k\Delta T(\vec{r},t) = F(\vec{r},t), \quad (14)$$

T is the temperature to be calculated, which is related to both time and space; F is the intensity of the heat source; k, ρ, and c are the thermal conductivity, density, and specific heat capacity, respectively.

Thermal convection follows the following equation,

$$q = h_f \left(T_s - T_B\right), \quad (15)$$

h_f is the surface heat transfer coefficient, T_s is the temperature of the surface of the object, T_b is the temperature of the surrounding fluid.

Inside the solid medium, the heat diffuses in the form of heat conduction. Between the antenna and the air, the heat diffuses in the form of thermal convection.

III. DISTRIBUTION CHARACTERISTICS OF ELECTRIC FIELD AND TEMPERATURE FIELD

In this work, the finite element software COMSOL was used to simulate and analyze the distribution characteristics of the electric field and temperature field at the end of VLF antenna.

A. Modelling of a VLF antenna in COMSOL

Although the total length of VLF antenna is 2km, the electric field is only distributed in multi-directional at the end of the antenna, and the electric field only exists along the normal direction in other parts. Therefore, when analyzing the distribution characteristics of electric field and temperature field, only the situation within 1m of the antenna end should be concerned.

Since the model of VLF antenna and improvement measures are relatively complex and difficult to implement in COMSOL Multiphysics. In this paper, the 3D design software SolidWorks is chosen to build the model and then import it into COMSOL Multiphysics for simulation calculation.

The simulation model of the antenna is shown in Fig. 3. The antenna structure in the simulation is the same as the antenna composition structure described in part A of Section II, and the diameters of antenna structure in tensile layer (aramid), inner sheath, antenna conductor (copper layer) and outer sheath layer are 15.4mm, 16.4mm, 17.0mm and 20.0mm respectively. Table 1 gives the relevant parameters of high-power VLF antenna material.

Table 1: Parameters of the material of the VLF antenna

Material	Relative Permittivity	Conductivity ($S \cdot m^{-1}$)
Inner sheath	2.2	1.0×10^{-14}
Copper	/	5.8×10^{7}
Outer sheath	2.3	2.0×10^{-12}
Aramid layer	3.3	1.0×10^{-14}
Air	1.0	2.0×10^{-12}

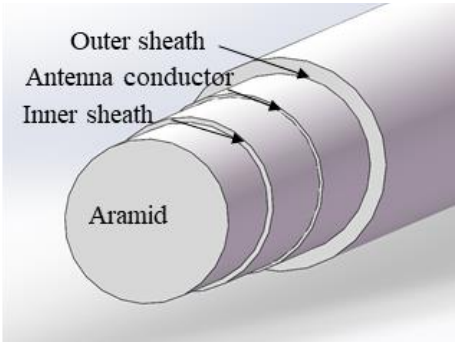

(a)

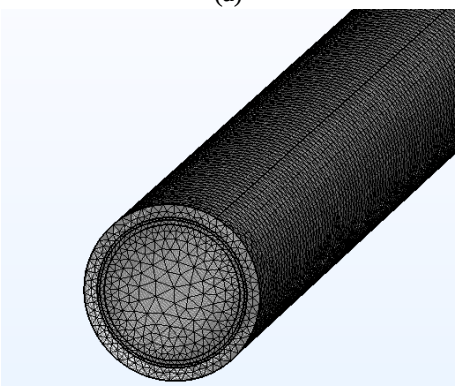

(b)

Fig. 3. The simulation model of the VLF antenna.

B. Distribution characteristics of electric field

According to the actual operating parameters of a high-power VLF communication system, the magnitude and frequency of the excitation voltage were set to U=120 kV and f=10 kHz in simulation. The obtained electrical field distribution at the terminal of the high-power VLF antenna is visualized in Fig. 4.

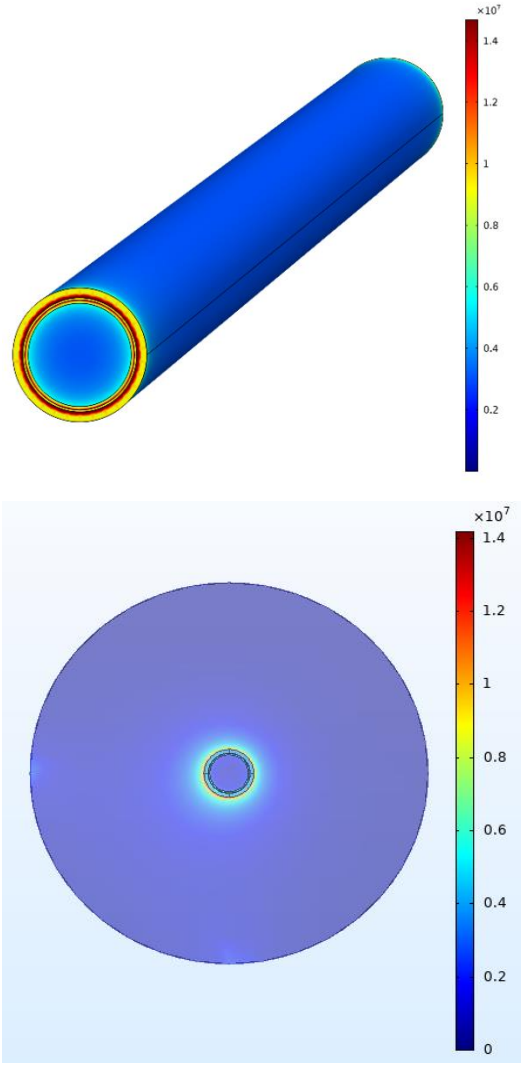

Fig. 4. Distribution of electric field at the end of the VLF antenna.

It can be observed from Fig. 4 that the electric field at the terminal of the antenna is distributed symmetrically about the axis in the radial direction. The electric field intensity of the copper layer is the maximum, and the electric field intensity in the outer sheath shows a decaying trend from the inside to the outside. Furthermore, the electric field intensity of the inner sheath and the aramid layer decreases from the copper layer to the axis, which is lower than the electric field intensity of the outer sheath.

In addition, Fig. 5 shows the radial distribution curve of the electric field at the terminal of the VLF antenna. It can be seen that the electric field intensity of the copper layer at the terminal of the antenna is highest, up to 1.4×10^7 V/m, and it is much higher than the corona inception field intensity of the air (about 3×10^6 V/m). In this case, air would be ionized, and corona discharge occurs. Meanwhile, the electric field intensity decreased from 1.4×10^7 V/m to 7.0×10^6 V/m within the thickness of the outer sheath. Although the electric field intensity decreases significantly to about half of its original value, it is still higher than the corona inception field intensity in the air.

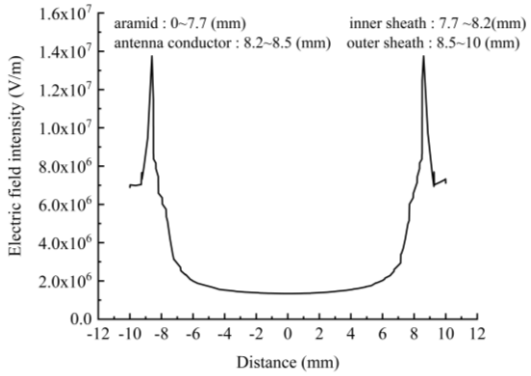

Fig. 5. The radial distribution of the electric field at the terminal of antenna.

C. Distribution characteristics of temperature field

In order to study the distribution characteristics of the temperature field at the terminal of the VLF antenna, in this case, the magnitude and frequency of the excitation voltage were set so U=120 kV and f=30 kHz, and the initial temperature is T=40℃. The properties of antenna material are given in Table II. In this case, the outer sheath material is Polyethylene. The distribution of the temperature field at the terminal of the VLF antenna was obtained and the result is shown in Fig. 6.

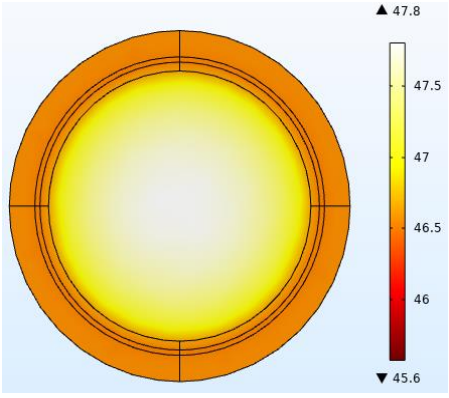

Fig. 6. Temperature distribution at the VLF antenna end.

Table 2: Material properties of antenna

Material	Relative Permittivity	tan δ	Thermal Conductivity W/ (K·m)	Heat Capacity kJ/ (K kg)
Inner sheath	2.2	5.0×10^{-4}	0.48	2.2
Aramid	3.3	8.0×10^{-4}	0.2	1.0
Polyethylene (PE)	2.3	2.0×10^{-4}	0.48	2.3
Polyvinyl chloride (PVC)	2.0	1.0×10^{-2}	0.17	1.0
Ethylene propylene rubber (EPDM)	3.1	3.0×10^{-3}	0.23	1.4

It can be clearly seen from Fig. 6 that the temperature field at the terminal of the antenna is symmetrically distributed about the axis, and the highest temperature is at the center of the aramid layer, which is 47.8℃, raised by 7.8℃ from its initial temperature. Meanwhile, the average temperature rise of the inner sheath is 6.6℃. Furthermore, the temperature rises of the outer sheath layer and the inner sheath layer are close, as can be observed from Fig. 6.

IV. INFLUENCING FACTORS OF ELECTRIC FIELD AND TEMPERATURE

In this section, the effects of excitation source characteristics, diameter of the antenna conductor, and material properties on electric field and temperature field are studied.

A. Influence of excitation source

1) The effect of voltage amplitude

During normal operation, the excitation voltage of the high-power VLF antenna is loaded from the feed window at the bottom of the antenna. According to the actual operating conditions of high-power VLF communication system, the range of excitation voltage is from 20 kV to 120 kV. The maximum electric field intensity value at the end of the VLF antenna are obtained by simulation calculation with f=10 kHz. The relationship between the magnitude of the excitation voltage and the electrical field intensity is shown in Fig. 7.

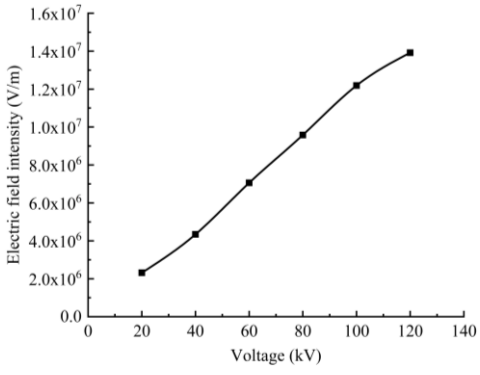

Fig. 7. Relationship between the maximum electric field intensity and the excitation voltage.

It can be seen from Fig. 7 that the electric field intensity at the end of the antenna increases nearly linearly with increased excitation voltage amplitude. The minimal electric field intensity at the end of the antenna is 2.0×10^6 V/m when the excitation voltage amplitude is 20 kV, and the maximum electric field intensity is 1.39×10^7 V/m at 120 kV, which increases by nearly seven times.

In addition, the influence of excitation source voltage amplitude on the temperature field at the end of the antenna with different outer sheath materials is investigated. Figure 8 shows the variation of temperature over time of different outer sheath materials under different magnitudes of the excitation voltage.

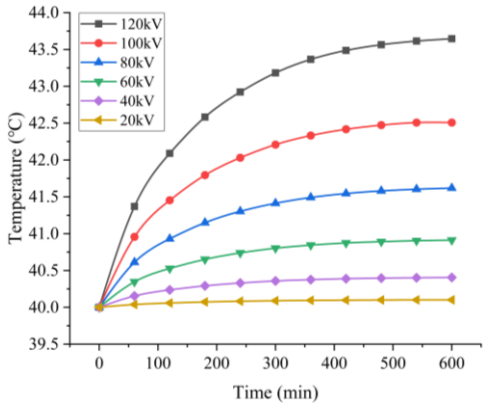

(a)

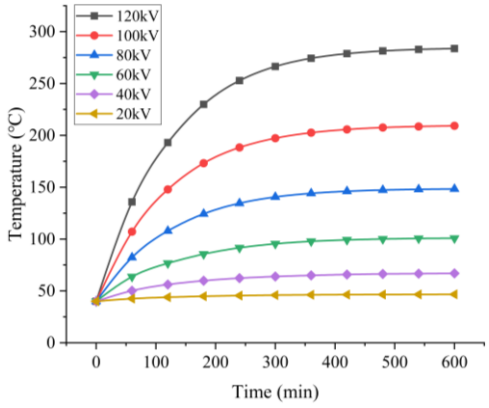

(b)

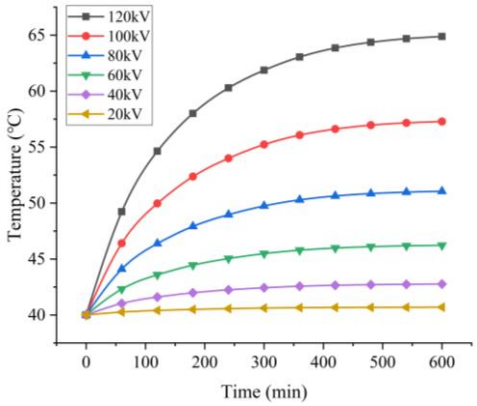

(c)

Fig. 8. Temperature rises at the terminal of VLF antenna under different voltage: (a) polyethylene; (b) polyvinyl chloride; (c) ethylene propylene rubber.

Some interesting relationships and characteristics can be observed from Fig. 8. First, the temperature at the end of the VLF antenna increases with increased loading excitation time. When the excitation voltage amplitude is small, the generated heat loss of the medium is not significant, and the thermal equilibrium is reached quickly. As excitation voltage amplitude increases, the heat loss increases gradually.

Second, for the same outer sheath material, the temperature at the end of the VLF antenna increases with increased excitation voltage amplitude. At the same time, the higher the excitation voltage amplitude is, the greater the temperature rise is at the end of the VLF antenna.

Third, under the same excitation voltage amplitude, polyvinyl chloride material has the most significant temperature rise, followed by ethylene propylene rubber, while the temperature rising of the polyethylene materials is the least. When the excitation voltage amplitude is U=120kV, the temperature rises of the three materials are 240℃, 25℃ and 3.75℃, respectively. The corresponding temperature growth rates of different materials are 600%, 62.5% and 9.4%, respectively. This is because the tangent of the dielectric loss Angle of polyethylene is much larger than that of the other two kinds of material.

2) The effect of frequency of the excitation source

In order to study the influence of the frequency of the excitation source on the electric field distribution at the end of the VLF antenna, in this case simulation was conducted by varying frequency from 3 kHz to 30 kHz, and the amplitude of the excitation voltage is set to 120 kV. The simulation results are shown in Fig. 9.

The Fig. 9 shows that the maximum electric field intensity at the terminal of the VLF antenna maintains almost a constant of 1.38×10^7 V/m with varying frequencies. This shows that the frequency of excitation source has little influence on the maximum value of the electric field intensity at the end of the antenna. Therefore, it is reasonable to consider the electromagnetic field in the VLF range as an electric quasi-static field.

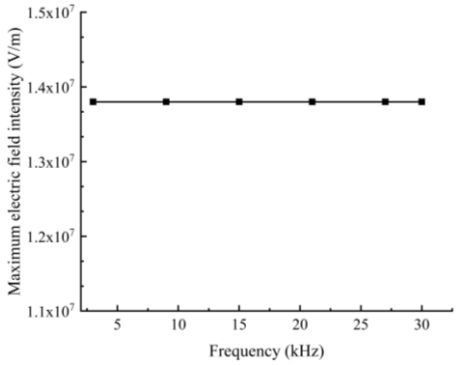

Fig. 9. Maximum electric field intensity with frequency.

Next, to investigate the effect of frequency on the temperature field, the initial temperature is 40℃ and other calculation conditions remain unchanged. The results were obtained and shown in Fig. 10.

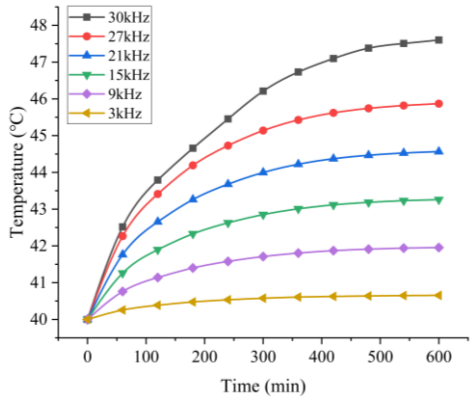

(a)

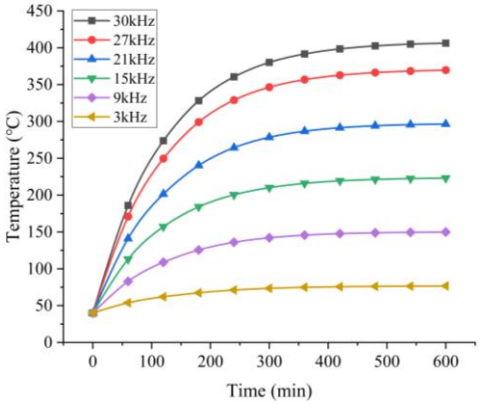

(b)

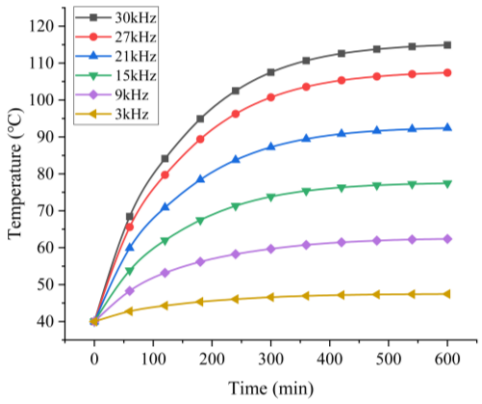

Fig. 10. Temperature rises at the terminal of VLF antenna under different frequency: (a) polyethylene; (b) polyvinyl chloride; (c) ethylene propylene rubber.

According to the simulation results, it can be seen that, first, the temperature at the VLF antenna end increases with increasing of the excitation source loading time. When the frequency of the excitation source is smaller, the heat of the dielectric loss of the material in the alternating electric field is small, and the time to achieve thermal equilibrium is short. With increasing of the frequency of the excitation source, the heat of the dielectric loss is larger.

Second, when the frequency is the same, the temperature rising of polyethylene is smaller, and polyvinyl chloride is the most significant. When the frequency of the excitation source was 30 kHz, the temperature rising of polyvinyl chloride reached 360°C, increasing by 900%; the ethylene-propylene rubber increases by 75°C, an increase of 187%; while the temperature rise of polyethylene is only 8°C, which increases by 20%.

B. Influence of the diameter of the antenna conductor

In this sub-section, the influence of diameter of the antenna conductor on the electric field at the end of the VLF antenna is studied. In simulation, the range of diameter of the antenna conductor is set from 0.05 mm to 1.3 mm, and the step change is 0.25 mm. The electric field intensity under different diameter of the antenna conductor were obtained, and the results are shown in Fig. 9.

It can be seen from Fig. 11 that when the diameter of the antenna conductor increases from 0.05 mm to 1.3 mm, the maximum electric field intensity at the end of the VLF antenna decreases with the increasing of the diameter of the antenna conductor. From 0.05 mm to 0.55 mm, the maximum value of the electric field intensity at the end of the antenna decreases significantly, whereas from 0.55 mm to 1.3 mm, the rate of decrease of the electric field intensity gradually slows down. When the diameter of the antenna conductor increases from 0.05 mm to 1.3 mm, the maximum electric field intensity at the terminal of antenna decreases from 1.41×10^7 V/m to 5.73×10^6 V/m with a drop of 59.4%.

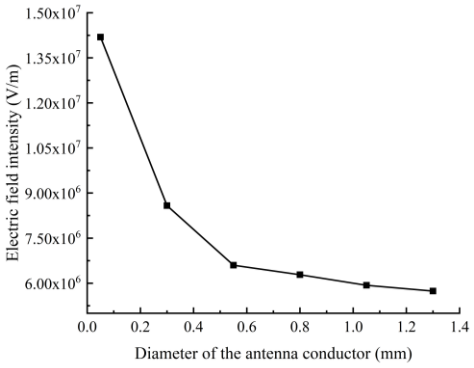

Fig. 11. Electric field intensity with the diameter of the antenna conductor.

It can be also seen from Fig. 11 that the electric field intensity will be affected by changing of the diameter of the antenna conductor. According to the analysis in Section II, the power of the dielectric loss is directly proportional to the square of the electric field intensity. Hence, changing of the diameter of the antenna conductor will affect the distribution of temperature field at the end of the antenna. The corresponding simulation results are shown in Fig. 12 and Fig. 13.

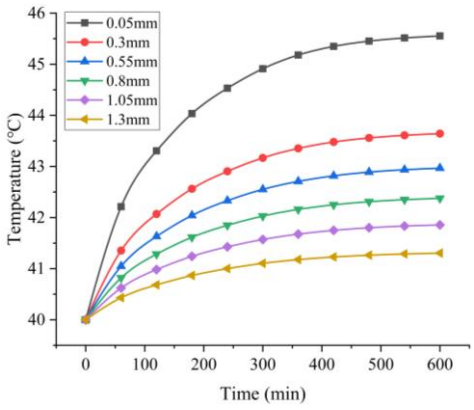

Fig. 12. Temperature rising of polyethylene with different conductor diameter.

As can be seen from Fig. 12 and Fig. 13:

(1) The temperature rising at the end of the VLF antenna increases with increasing excitation time. At the same time, the thicker the copper layer is, the smaller the temperature rise at the end of the VLF antenna is.

(2) The temperature rise at the end of the VLF antenna is negatively proportional as the diameter of the antenna conductor increasing in same moment.

(3) When the diameter of the antenna conductor is 1.3mm, the temperature rising to reach thermal equilibrium is only about 1℃. However, when the diameter of the antenna conductor is 0.05mm, the temperature rise is close to 5.5℃, which increases by 450% compared with the diameter of 1.3mm.

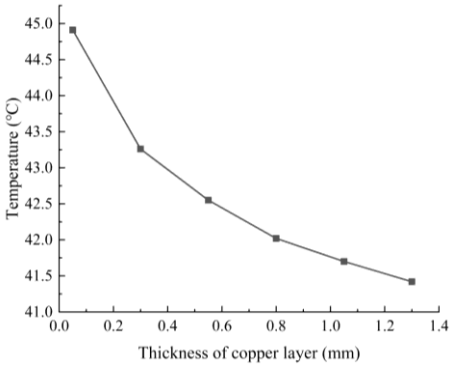

Fig. 13. Temperature rising with thickness of copper layer.

C. Influence of the material properties of outer sheath

It can be seen from Equation (13) that the dielectric loss power is related to the material properties. Therefore, it is necessary to investigate the material properties of the outer sheath of the antenna. The materials in Table 2 are selected for simulation research in this paper.

1) The effect of material conductivity on the electric field

The effect of material conductivity on the electric field is studied in this section. Setting the range of conductivity of the outer sheath material is from 10^{-12} S • m^{-1} to 10 S • m^{-1}. The simulation results are shown in Fig. 14.

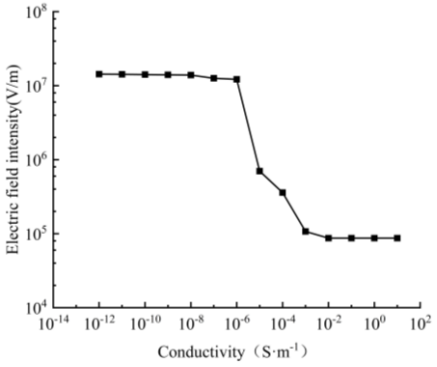

Fig. 14. The curve of electric field intensity with conductivity.

According to Fig. 14:

(1) The electric field intensity at the end of the VLF antenna decreases with the increasing of the conductivity when the conductivity of the outer sheath material changes from 10^{-12} S • m^{-1} to 10 S • m^{-1}. The electric field intensity decreased significantly from 1.43×10^{7} V/m to 8.7×10^{4} V/m.

(2) When the conductivity of the outer sheath material is less than 10^{-6} S·m^{-1}, the amplitude of the electric field intensity at the end of the antenna changes less. whereas the electric field intensity significantly decreased when the outer sheath conductivity increases from 10^{-6} S·m^{-1} to 10^{-2} S·m^{-1}. Continuing to increase the conductivity, the electric field intensity is almost unchanged.

2) The effect of material properties on temperature field

In order to study the influence of different material parameters of outer sheath on the temperature field, setting U=120 kV, f=10 kHz, and the initial temperature T=40°C to obtain the maximum temperature rise of different materials, as shown in Fig. 15.

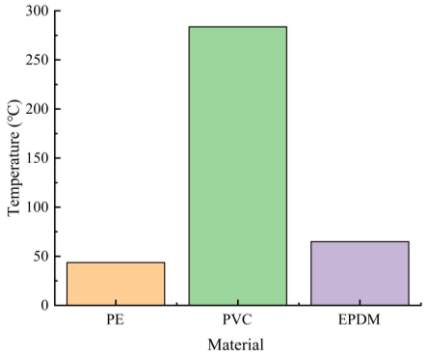

Fig. 15. The curve of temperature rising in different materials.

It can be seen from Fig. 15 that temperature rise exists in all three materials, of which temperature rising of polyvinyl chloride is the most significant, reaching 240℃, followed by ethylene propylene rubber, while the temperature rising of polyethylene is less than 10℃. In addition, the temperature rise of polyvinyl chloride has far exceeded its softening temperature 85℃, so it cannot be used as the outer sheath material, and the other materials meet the requirements.

Similar research has been conducted by Dong of the Wuhan Ship Communication Research Institute [22]. In their simulations on the CST software, the maximum temperature calculations on polyethylene, polyvinyl chloride and ethylene propylene rubber were 41℃, 794℃ and 60℃ when the voltages were all 100 kV/20kHz, respectively. The results of this paper are basically consistent with the results of Dong's, but the simulation results on PVC material are more different. The possible

reason is that the $tan\delta$ setting of PVC is different.

V. ELECTRIC FIELD IMPROVEMENT AND TEMPERATURE RISE SUPPRESSION

Based on the analysis results from the previous section, in order to improve the electric field distribution and suppress the severe temperature rise at the end of the VLF antenna, a dielectric loss eliminator is designed and the effectiveness of the device is verified by simulation.

A. Modelling of a dielectric loss eliminator

In view of the electric field distortion and temperature rise at the end of the VLF antenna, dielectric loss eliminator is designed, which is used to achieve the electric isolation between the antenna and the floating platform, to reduce the electric field intensity, to eliminate the dielectric loss and to suppress the temperature rise [23-25]. Figure 16 shows the schematic diagram of the dielectric loss eliminator. The parameters of the dielectric loss eliminator are shown in Table 3.

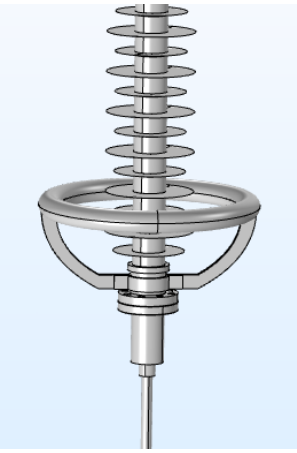

Fig. 16. Schematic diagram of dielectric loss eliminator.

Table 3: Parameters of the dielectric loss eliminator

Tube Radius/mm	Corona Ring Radius/mm	Corona Ring Height
20	200	172.6

The process of solving the equation using the finite element method requires the determination of the definite solution of the equation based on the boundary conditions of the field. The edge value problem at the end of the VLF antenna in this paper is summarized by the constraint equations:

$$\begin{cases} \nabla^2\varphi = -\dfrac{\rho}{\varepsilon^{'} - i\varepsilon^{''}} \\ \varphi = \varphi(x, y, z) \\ \varphi(r)\,|_{r\to\infty} = 0 \\ ((\varepsilon_1^{'} - i_1^{''})\dfrac{\partial\varphi}{\partial n}) - ((\varepsilon_2^{'} - i_2^{''})\dfrac{\partial\varphi}{\partial n}) = \sigma. \end{cases} \tag{16}$$

In order to refine the calculation as much as possible within the range that the computer can bear, the mesh size is set to 1mm.

B. Electric field improvement by dielectric loss eliminator

The improvement effect of the electric field is analyzed after adding the dielectric loss eliminator. Setting the calculation conditions: U=120 kV and f=10 kHz. The electric field distribution with the dielectric loss eliminator is shown in Fig. 17.

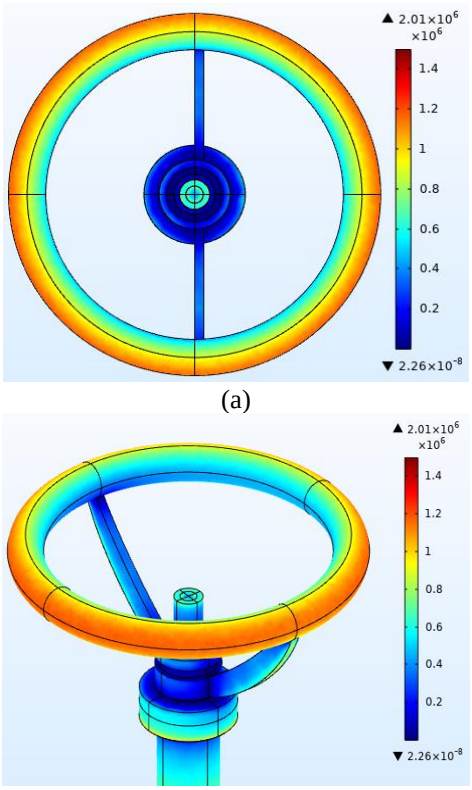

(a)

(b)

Fig. 17. Distribution of electric field at the terminal of VLF antenna: (a) vertical view; (b) front view.

Compared to Fig. 4, it can be seen from Fig. 17 that the electric field intensity on the outer surface of the dielectric loss eliminator is the highest. After increasing the dielectric loss eliminator, the electric field intensity of the antenna system is significantly reduced, and the maximum electric field intensity is only 2.01×106 V/m, which indicates that the dielectric loss eliminator has a significant effect on the improvement of the electric field intensity at the antenna end.

Figure 18 shows the radial distribution of the electric field at the end of the VLF antenna after increasing the dielectric loss eliminator. It can be seen from Fig. 18 that:

(1) The maximum electric field intensity at the end of the VLF antenna is 1.57×10^6 V/m, which is smaller than the corona field intensity of air.

(2) The electric field intensity gradually decreases in the air domain. In the range of radial distance from - 9.25 mm to + 9.25 mm, the electric field intensity decreases from 1.57×10^6 V/m to 4.4×10^5 V/m, which decreases about 72%, and the electric field intensity at the axis is the lowest.

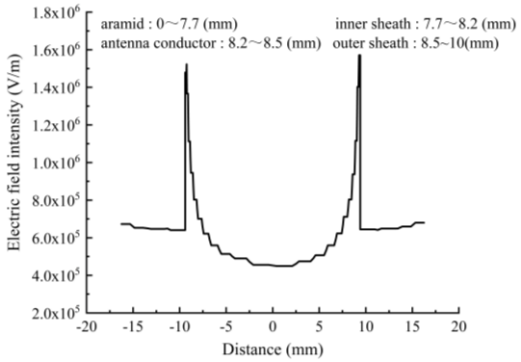

Fig. 18. Radial distribution curve of the electric field at the antenna end.

C. Temperature rise suppression by dielectric loss eliminator

According to the above analysis, the electric field intensity at the terminal of the antenna is improved to a great extent by using the dielectric loss eliminator. Theoretically, the antenna end is in an alternating electric field, and the heating power caused by the dielectric loss is directly proportional to the square of the electric field intensity, so the significant reduction of the electric field intensity will have an obvious inhibitory effect on the temperature rise of the antenna end. The following carries out the simulation calculation of the temperature field at the terminal of the antenna to analyze the temperature rise inhibition effect after adding dielectric loss eliminator. Setting the U=120 kV, f=10 kHz, and the initial temperature T=40℃. The distribution characteristics of the temperature field at the terminal of the VLF antenna is obtained by simulation calculation, as shown in Fig. 19.

As can be seen from Fig. 19:

(1) The temperature of the metal parts at the end of the antenna barely changes because the current at the terminal of the antenna is zero and there is no Joule heat.

(2) There is a temperature rise phenomenon at the connection between the dielectric loss eliminator and the epoxy core rod. The maximum temperature is 40.8℃, and the temperature rise is 0.8℃, which is caused by the dielectric loss of the epoxy core rod in the alternating field. However, when the dielectric loss eliminator is adopted, the electric field intensity has obviously decreased, so the temperature rise is very small.

(3) The electrical performance parameters of the epoxy core rod are similar to ethylene propylene rubber materials. That is to say, the dielectric constant and tangent of the loss angle of epoxy core rod are similar to ethylene propylene rubber. In Section IV, under U=120 kV and f=10 kHz, the temperature rise of ethylene propylene rubber exceeds 20℃, while the temperature rise of the epoxy core rod is only 0.8℃. It can be concluded that the temperature rise at the terminal of the VLF antenna can be significantly suppressed by using the dielectric loss eliminator.

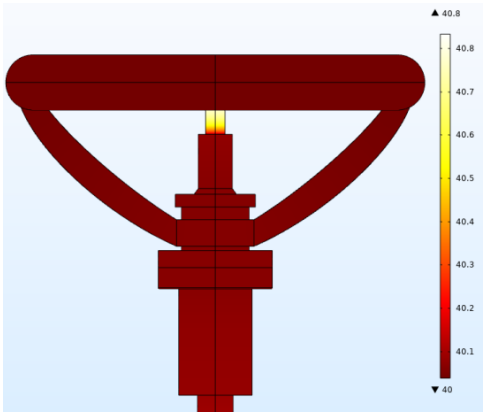

Fig. 19. Cloud diagram of temperature rise.

VI. CONCLUSION

The distribution characteristics and values of the electric field and temperature field at the end of VLF antenna are obtained by the simulation calculation. The effects of the excitation source, the diameter of the antenna conductor, and the material properties of the outer sheath of the antenna on the electric field are studied. It is found that the electric field intensity at the terminal of the VLF antenna increases with increased magnitude of the excitation voltage, whereas the frequency of the excitation has no effect on the electric field. The diameter of the antenna conductor is negatively related to the electric field intensity. In addition, the temperature at the terminal of the VLF antenna is positively correlated with the magnitude and the frequency of the excitation voltage, and the influence of the outer sheath material on the temperature rise is significant.

A dielectric loss eliminator is designed to improve the electric field distribution and suppress the temperature rise, and the effect of the designed device is verified to be very significant by simulation. In practice, the use of the dielectric loss eliminator can effectively avoid VLF antenna breakage accidents due to temperature rise.

REFERENCES

[1] M. L. Burrows, "ELF communications antennas," *IEEE Electromagn. Wave*, vol. 24, no. 11, pp. 863, May 1978.

[2] L. B. Pedersen, L. Persson, and M. Bastani, "Airborne VLF measurements and mapping of ground conductivity in Sweden," *J. Appl. Geophys.*, vol. 67, no. 3, pp. 250-258, Nov. 2007.

[3] T. A. Miś, "The concept of an airborne VLF transmitter with vertical electric dipole antenna," in *Symposium on Antennas and Propagation & USNC/URSI National Radio Science Meeting*, Boston, MA, pp. 1667-1668, 2018.

[4] L. L. Klessig and V. L. Strite, "The ELF odyssey: National security versus environmental protection," *Environ. Hist. Rev.*, vol. 6, no. 2, pp. 126-128, Oct. 1980.

[5] Z. W. Jin, "VLF/SLF wave propagation and its application on communication and navigation for submarine," *Equip. Environ. Eng.*, vol. 5, no. 3, pp. 57-61+86, Apr. 2008.

[6] C. F. Zhan, "Discussion on the technical methods of geological and mineral exploration," *China Standardization*, vol. 5, no. 11, pp. 121-122, Jan. 2019.

[7] J. J. Doherty, "Submarine communication," *J. Acoust. Soc. Amer.*, vol. 69, no. 1, pp. 335, Nov. 1981.

[8] R. Barr, D. L. Jones, and C. J. Rodger, "ELF and VLF radio waves," *J. Atmos. Sol.-Terr. Phys.*, vol. 62, no. 17, pp. 1689-1718, June 2000.

[9] T. S. Zhang, Z. Z. Xu, and M. H. Zheng, "Application of VLF electromagnetic method in ore body spatial location prediction," *Geol. Sci. Technol. Inormat.*, vol. 18, no. 4, pp. 85-88, Dec. 1999.

[10] Y. Wei, "A communication system application based on floating platform," *Communication & Information Technology*, vol. 186, no. 4, pp. 72-74, Dec. 2010.

[11] H. C. Koons and M. H. Dazey, "High-power VLF transmitter facility utilizing a balloon lofted antenna," *IEEE Transactions on Antennas and Propagation*, vol. 31, no. 2, pp. 243-248, 1983.

[12] R. Cuggia, J. L. Dubard, and M. Ney, "Numerical characterization of insulators for VLF antennas," *Annual Review of Microbiology*, vol. 6, no. 6, pp. 207-208, 2009.

[13] T. H. Deng, C. Liu, and J. Zhang, "High voltage insulator for high power VLF transmitting antenna," *Ship Electron. Eng.*, vol. 36, no. 5, pp. 168-171, May 2016.

[14] Y. Liu, F. S. Deng, H. Q. Sun, W. Zha, J. Liu, and T. Cao, "Electromagnetic characteristics of airborne dual trailing antenna for the submarine communication," in *Proc. 2018 Int. Appl. Comput. Electromagn. Soc. Symp. - China (ACES)*, Beijing, China, pp. 1-2, 29 July-1 Aug. 2018.

[15] L. Yong, D. Fangshun, S. Hengqing, W. Qisi, and S. Liyuan, "Simulation on the electromagnetic environment in the carrier of airborne VLF wire antennas," in *Proc. 2018 IEEE Int. Conf. Comput. Electromagn. (ICCEM)*, Chengdu, China, pp. 1-3, 26-28 Mar. 2018.

[16] J. Chen, D. Su, Y. Liu, and N. Wu, "Simulation analysis of airborne VLF Wire Antennas based on FEM," in *Proc. 2011 Int. Conf. Electron., Commun. Control (ICECC)*, Ningbo, China, pp. 2276-2279, 9-11 Sep. 2011.

[17] R. Cuggia, J. L. Dubard, M. Ney, and C. Pichot, "Numerical characterization of insulators for VLF antennas," in *Proc. 2009 3rd European Conf. Antennas Propag.*, Berlin, Germany, pp. 1570-1572, 2009.

[18] F. Yang, X. X. Wu, S. M. Chen, and L. Fang, "Characteristics of dielectric loss and electric field homogenization at the terminal opening of high power communication antenna," *Chinese J. Radio Sci.*, vol.33, no. 2, pp. 162-169, May 2018.

[19] J. G. Zhou, "A calculation method of very low frequency transmitting antennas corona voltage," *Telecom Power Technol.*, vol. 31, no. 4, pp. 49-51, Apr. 2014.

[20] K. Mao, X. Li, C. Wei, Z. Ma, and X. Wu, "Numerical analysis of electric field distribution at the terminal of VLF antenna," in *Proc. 2019 IEEE 19th Int. Conf. Commun. Technol. (ICCT)*, Xi'an, China, pp. 819-822, 2019.

[21] X. Y. Shi, Y. B. Wang, B. Huang, and M. Xie, "Research on the safety protection distance of electromagnetic radiation for high power very low frequency antenna array," *Ship Electron. Eng.*, vol. 39, no. 12, pp. 199-203, Dec. 2019.

[22] J. Dong and J. X. Luo, "Analysis of VLF balloon antenna cable terminal loss and heating-up," *Ship Electron. Eng.*, vol. 35, no. 12, pp. 159-161, Dec. 2015.

[23] J. Yang. "Research on effectiveness evaluation of long wave VLF communication system," *Information System Engineering*, pp. 24, Sep. 2018.

[24] L. S. Huang and Y. Z. Jiang. "Matrix quantity method study on the performance of VLF balloon antenna," *Modern Communication Technology*, vol. 001, pp. 17-21, 2005.

[25] Z. G. Zhang. "Research on VLF horizontal low frame transmitting antenna technology," *China Academy of Naval Research*, MS, 2012.

[26] B. M. Hamdi, M. Teguar, and A. Mekhaldi. "Optimal design of corona ring on HV composite insulator using PSO approach with dynamic population size," *IEEE Transactions on Dielectrics and Electrical Insulation*, vol. 23, no. 2, pp. 1048-1057, 2016.

Xianqiang Li (M'17) was born in Xiangyang, China in 1973. He received the B.S., M.S. and Ph.D. degrees in High Voltage and Insulation Technology from Wuhan University, Wuhan, China, in 1995, 1998 and 2015, respectively. He is currently a Lecturer of the Electrical Engineering Department of Wuhan University of Technology, Wuhan, China. His research interests include lightning protection and grounding technology, transformer modeling, external insulation of electrical equipment and substation live working.

Kedan Mao was born in Leshan, China in 1994. He received the B.E. and M.S. degrees in 2018, and 2020, respectively. He is currently an Assistant Engineer of the Nuclear Power Institute, Chengdu, China. His research interests in external insulation of electrical equipment.

Ao Wang was born in Wuhan, China in 1996. He received the B.Sc. degree in Mechanical Design Manufacture and Automation from Jianghan University, Wuhan, China. He is pursuing the M.Sc. degree in the School of Automation, Wuhan University of Technology right now. His research interests are electrical theory and new technology.

Ji Tian was born in Hubei, China in 1997. He received the B.Sc. degree in Electrical Engineering from China Three Gorges University, Yichang, China, in 2019. At present, he is pursuing the M.Sc. degree in the School of Automation, Wuhan University of Technology. His research areas are mainly on high voltage technology and electrical insulation.

Wenchuang Zhou was born in Huanggang, China in 1997. He received the B.Sc. degree in Automation from Hubei University of Technology, Wuhan, China, in 2018. At present, he is pursuing the M.Sc. degree in the School of Automation, Wuhan University of Technology. His research interests are high voltage, insulation and laser cleaning insulator contamination.